

# Measurement report: High contribution of N<sub>2</sub>O<sub>5</sub> uptake to particulate nitrate formation in NO<sub>2</sub>-limited urban areas

Ziyi Lin<sup>1,2,3</sup>, Chuanyou Ying<sup>4</sup>, Lingling Xu<sup>1,2\*</sup>, Xiaoting Ji<sup>1,2,3</sup>, Keran Zhang<sup>1,2</sup>, Feng Zhang<sup>2</sup>, Gaojie Chen<sup>1,2,3</sup>, Lingjun Li<sup>1,2,3</sup>, Chen Yang<sup>1,2,3</sup>, Yuping Chen<sup>1,2,3</sup>, Ziyang Chen<sup>1,2,3</sup>, Jinsheng Chen<sup>1,2\*</sup>

## Affiliations:

<sup>1</sup>State Key Laboratory of Advanced Environmental Technology, Institute of Urban Environment, Chinese Academy of Sciences, Xiamen 361021, China

<sup>2</sup>Fujian Key Laboratory of Atmospheric Ozone Pollution Prevention, Institute of Urban Environment, Chinese Academy of Sciences, Xiamen 361021, China

<sup>3</sup>University of Chinese Academy of Sciences, Beijing 100049, China

<sup>4</sup>Fuzhou Institute of Environmental Science, Fuzhou 350013, China

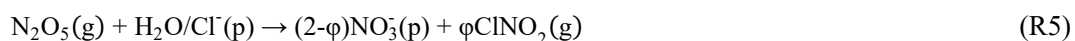
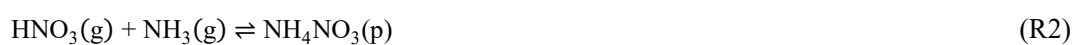
\*Correspondence to: Jinsheng Chen (jschen@iue.ac.cn); Lingling Xu (linglingxu@iue.ac.cn)

**Abstract:** Particulate nitrate (pNO<sub>3</sub><sup>-</sup>) is a major component of fine particles in Chinese urban areas. However, the relative contributions of pNO<sub>3</sub><sup>-</sup> formation pathways in urban areas remain poorly quantified, particularly under the NO<sub>2</sub>-limited regime that governs its formation (as defined by the NO<sub>2</sub>/O<sub>3</sub> ratio), which hinders effective particulate pollution control. In this study, comprehensive winter field observations were conducted in urban Xiamen, Southeast China. We observed significantly elevated nighttime pNO<sub>3</sub><sup>-</sup> levels concurrent with increased N<sub>2</sub>O<sub>5</sub> concentrations. Quantification using an observation-constrained model revealed that N<sub>2</sub>O<sub>5</sub> uptake contributed 51.2% to total pNO<sub>3</sub><sup>-</sup> formation, which was comparable to that of the OH + NO<sub>2</sub> reaction. The N<sub>2</sub>O<sub>5</sub> uptake was found to be mainly driven by nocturnal NO<sub>3</sub> oxidation capacity (modulated by NO<sub>2</sub> and O<sub>3</sub> levels) rather than by heterogeneous reaction conditions. Sensitivity simulations further demonstrated that pNO<sub>3</sub><sup>-</sup> formation rate was more sensitive to NO<sub>x</sub> variations than to VOCs variations. Implementing NO<sub>x</sub> control measures at nighttime was shown to effectively reduce pNO<sub>3</sub><sup>-</sup> by abating N<sub>2</sub>O<sub>5</sub> uptake while simultaneously preventing daytime O<sub>3</sub> increase. Our findings enhance the understanding of pNO<sub>3</sub><sup>-</sup> formation in NO<sub>2</sub>-limited urban areas and provide valuable insights for developing joint PM<sub>2.5</sub> and O<sub>3</sub> mitigation strategies.



## 1 Introduction

Fine particulate matter (PM<sub>2.5</sub>) contributes to various atmospheric environmental issues, including visibility deterioration, radiative forcing change, and adverse impacts on human health (Seinfeld, 1989; Lelieveld et al., 2015). Among its chemical components, particulate nitrate (pNO<sub>3</sub><sup>-</sup>) has attracted increasing attention due to its rising mass fraction in PM<sub>2.5</sub> and its nonlinear responses to emission mitigation strategies (Xie et al., 2022; Zhai et al., 2021; Li et al., 2021; Zhang et al., 2021; Zhou et al., 2022; Zong et al., 2022; Wang et al., 2020). The primary formation pathways of pNO<sub>3</sub><sup>-</sup> include gas-phase oxidation through the reaction of hydroxyl radicals (OH) and nitrogen dioxides (NO<sub>2</sub>) (R1–R2), and heterogeneous uptake of dinitrogen pentoxide (N<sub>2</sub>O<sub>5</sub>) which is produced via NO<sub>2</sub> oxidation by nitrate radicals (NO<sub>3</sub>) (R3–R5) (Brown and Stutz, 2012). It is well recognized that the OH + NO<sub>2</sub> reaction dominates in daytime, while N<sub>2</sub>O<sub>5</sub> uptake dominates in nighttime. During nocturnal pNO<sub>3</sub><sup>-</sup> formation, particulate chlorides can induce N<sub>2</sub>O<sub>5</sub> heterogeneous uptake to produce ClNO<sub>2</sub>, thereby competing with pNO<sub>3</sub><sup>-</sup> formation.



Many studies have focused on quantifying the potential formation pathways of pNO<sub>3</sub><sup>-</sup> in urban areas of China. In major urban agglomerations such as the Beijing-Tianjin-Hebei (BTH) region (Chen et al., 2020; Ma et al., 2023; Zhao et al., 2023), Yangtze River Delta (YRD) (Sun et al., 2022; Zhai et al., 2023; Zhang et al., 2023b), and Pearl River Delta (PRD) (Yang et al., 2022; Niu et al., 2022; Cheng et al., 2024), pNO<sub>3</sub><sup>-</sup> formation was typically dominated by the gas-phase oxidation of OH + NO<sub>2</sub>. In contrast, under special conditions such as the COVID-19 pandemic and PM<sub>2.5</sub> pollution events (Yan et al., 2023; Zhai et al., 2023), N<sub>2</sub>O<sub>5</sub> uptake became the main pathway. Previous research has demonstrated that the formation rate of pNO<sub>3</sub><sup>-</sup> via N<sub>2</sub>O<sub>5</sub> uptake is closely related to its precursor NO<sub>2</sub> and O<sub>3</sub>, and the N<sub>2</sub>O<sub>5</sub> formation can be classified into NO<sub>2</sub>-limited and O<sub>3</sub>-limited regimes based on the NO<sub>2</sub>/O<sub>3</sub> ratio (Ma et al., 2023). The winter NO<sub>2</sub>/O<sub>3</sub> ratios in the BTH, YRD, and PRD regions were generally above 1, placing N<sub>2</sub>O<sub>5</sub> formation



in the  $O_3$ -limited or transition regime (Ma et al., 2023; Wen et al., 2018; Li et al., 2021; Zhang et al., 2023b). However, the  $N_2O_5$  uptake served as the dominant pathway for  $pNO_3^-$  formation, typically under  $NO_2$ -limited conditions (e.g., reduced emissions during the pandemic) or under large aerosol surface areas (e.g., severe particulate pollution episodes). Collectively, these findings indicate that spatial variations in  $NO_2$  and  $O_3$  levels are likely a key driver of regional differences in the dominant formation pathways of  $pNO_3^-$ . The formation of  $pNO_3^-$  primarily depends on precursors OH,  $NO_2$ , and  $O_3$ , with OH and  $O_3$  concentrations being influenced by VOCs and  $NO_x$  emissions. Thus, the different formation pathways of  $pNO_3^-$  result in complex responses to  $NO_x$ /VOCs emissions. The response of  $pNO_3^-$  formation via  $OH + NO_2$  to precursors variation is relatively well-understood, as most Chinese urban areas are located in VOC-limited regimes for  $O_3$  (Wang et al., 2023a; Wang et al., 2022c; Zhang et al., 2023a; Mao et al., 2022), and ammonia-rich regimes for  $pNO_3^-$  (Xing et al., 2018; Sun et al., 2022; Fu et al., 2024; Liu et al., 2019). Under these conditions, VOCs reduction suppresses  $pNO_3^-$  formation by decreasing OH concentrations, whereas  $NO_x$  reduction enhances  $pNO_3^-$  formation by weakening the  $NO_x$  titration effect. Given the regional variations in the  $NO_2/O_3$  ratio across urban areas of China (Ma et al., 2023), the response of  $pNO_3^-$  formation via  $N_2O_5$  uptake to precursor changes (VOCs,  $O_3$ ) likely exhibits spatial heterogeneity. A recent study has revealed that under  $O_3$ -limited conditions for  $N_2O_5$  formation (Zhang et al., 2023b), reducing  $NO_x$  emissions had negligible effects, while reducing VOCs decreased the consumption of  $NO_3$  by VOCs, thereby enhancing  $pNO_3^-$  formation from  $N_2O_5$  uptake. However, the response of  $pNO_3^-$  formation to precursors under  $NO_2$ -limited conditions remains unclear. Aside from precursor availability,  $N_2O_5$  uptake is also greatly influenced by heterogeneous reaction conditions like aerosol composition and aerosol surface area (McDuffie et al., 2018b; McDuffie et al., 2018a; Tham et al., 2018; Yu et al., 2020), which introduces additional uncertainty in determining the contribution of  $pNO_3^-$  formation pathways and the effectiveness of precursor control strategies.

The  $NO_2/O_3$  ratios in southeastern China predominantly fell within the  $NO_2$ -limited regime for  $N_2O_5$  formation (Ma et al., 2023). Xiamen, as one of the most developed cities in southeastern China, exhibits relatively better air quality with low levels of VOCs and  $NO_x$  compared to China's megacities (**Table S1**). This pattern well represents the future urban atmospheric conditions following the implementation of air pollution control measures in China. From December 2022 to February 2023, we conducted comprehensive multi-parameter observations in urban Xiamen, including  $N_2O_5$  and related chemical constituents. An observation-constrained box model incorporating the heterogeneous reaction parameters



was utilized to quantify the rates of different  $\text{pNO}_3^-$  formation pathways. An explainable machine learning (ML) method was applied to identify the driving factors for high  $\text{pNO}_3^-$  formation rate via  $\text{N}_2\text{O}_5$  uptake. Additionally, multi-scenario simulations were performed to examine the joint responses of  $\text{pNO}_3^-$  and  $\text{O}_3$  formation to various  $\text{NO}_x$  and VOCs emissions. These findings enhance our understanding of  $\text{pNO}_3^-$  formation pathways and their environmental implications in  $\text{NO}_2$ -limited regions, providing valuable insights for developing joint  $\text{PM}_{2.5}$  and  $\text{O}_3$  mitigation strategies.

## 2 Methods

### 2.1 Field Observation.

Field observations were conducted during the winter period from 1 December 2022 to 3 February 2023, at an urban site (marked by the red star in **Figure S1**) in Xiamen, which is located in the southeastern coastal region of China. Detailed site information has been described in our previous studies (Yang et al., 2023; Liu et al., 2022). Trace gases (including PAN, HCHO, HONO, VOCs,  $\text{O}_3$ ,  $\text{NO}_x$ , CO, and  $\text{SO}_2$ ), chemical components in  $\text{PM}_{2.5}$  (including organic carbon and elemental carbon,  $\text{SO}_4^{2-}$ ,  $\text{NO}_3^-$ ,  $\text{NH}_4^+$ ,  $\text{Cl}^-$ ),  $\text{PM}_{2.5}$  mass concentration, and meteorological parameters (including ambient temperature (T), relative humidity (RH), atmospheric pressure (P), wind speed (WS), wind direction (WD), and photolysis rates) were continuously measured during the campaign. Detailed information about measurement methods and instruments is summarized in **Text S1**. In addition, boundary layer height (BLH) data were obtained from the ERA5 dataset (Hersbach et al., 2020).

A chemical ionization time-of-flight mass spectrometer equipped with an iodide source (iodide-TOF-CIMS, Aerodyne Research Inc., USA) was deployed to measure  $\text{N}_2\text{O}_5$  and  $\text{ClNO}_2$ . A nearly 2-meter long perfluoroalkoxy (PFA) tube with a 1/4-inch inner diameter was used for sampling. The total sampling flow rate was set as 10 standard liters per minute (SLPM), of which only 2SLPM was diverted to the CIMS. A nitrogen ( $\text{N}_2$ ) flow (99.999%, 2.7 SLPM), carrying methyl iodide ( $\text{CH}_3\text{I}$ ) vapor released from a heated permeation tube, passed through a soft X-ray source (Tofwerk AG, P-type) to generate reagent ions  $\text{I}^-$ . The  $\text{I}^-$  was combined with the target gas in an ion molecule reaction (IMR) chamber and then detected by the ToF-CIMS. Ambient  $\text{N}_2\text{O}_5$  and  $\text{ClNO}_2$  were detected as the  $\text{I}(\text{N}_2\text{O}_5)^-$  and  $\text{I}(\text{ClNO}_2)^-$  clusters at 235 and 208 m/z. The detailed calibration procedures of  $\text{N}_2\text{O}_5$  and  $\text{ClNO}_2$  are described in **Text S2**, following established methods (Wang et al., 2022b; Wang et al., 2022a; Thaler et al., 2011). Briefly,  $\text{N}_2\text{O}_5$  was generated from the reaction between  $\text{O}_3$  and excessive  $\text{NO}_2$ , while  $\text{ClNO}_2$  was



synthesized via the reaction of  $\text{Cl}_2$  (6 ppm in  $\text{N}_2$ ) with a moist mixture of  $\text{NaNO}_2$  and  $\text{NaCl}$ . The calibration curves for  $\text{N}_2\text{O}_5$  and  $\text{ClNO}_2$  at different RH are shown in **Figure S2**, with mean sensitivities of  $0.110 \pm 0.063$  and  $0.055 \pm 0.018$  ncps/ppb, respectively. The instrument background was determined by introducing dry  $\text{N}_2$  into the inlet for 20 min. Based on three times the standard deviation ( $3\sigma$ ) of the background signal, the typical 1-minute detection limits for  $\text{N}_2\text{O}_5$  and  $\text{ClNO}_2$  were estimated to be 1.3 and 0.61 ppt, respectively.

## 2.2 Determination of $\text{pNO}_3^-$ Formation Rate.

The iterative box model developed by Wagner et al. with a simplified mechanism was employed to obtain key parameters of the  $\text{N}_2\text{O}_5$  uptake process (Wagner et al., 2013), including the loss rate of  $\text{N}_2\text{O}_5$  ( $k\text{N}_2\text{O}_5$ ) and the production yield of  $\text{ClNO}_2$  ( $\phi\text{ClNO}_2$ , see in **Text S3**). To validate the iterative box model results, these parameters were calculated concurrently based on the classical steady-state approximation method (**Text S4**) (Brown et al., 2003; Chen et al., 2022). The derived parameters of  $\text{N}_2\text{O}_5$  uptake were adopted for subsequent multiphase box model.

A Framework for 0-D Atmospheric Modeling (F0AM), incorporating the Master Chemical Mechanism (MCM v3.3.1) and heterogeneous mechanisms (**Table S2**), was employed to simulate nitrate formation rates for each day during the study period (Wolfe et al., 2016; Atkinson and Arey, 2003; Jenkin et al., 2015). The heterogeneous parameters derived from the iterative box model were implemented in F0AM. In addition, hourly interval data of trace gases, photochemically active species, meteorological variables, and reanalysis data were also applied to constrain the multiphase chemical box model. Detailed model configurations are provided in **Text S5**. As shown in **Figure S3**, the model performed well in simulating the trends of  $\text{N}_2\text{O}_5$  and  $\text{ClNO}_2$  with  $R^2$  of 0.88 and 0.49, respectively. However, a systematic underestimation existed in the simulated  $\text{N}_2\text{O}_5$  and  $\text{ClNO}_2$  concentrations, which likely resulted from the model configuration including overestimated physical removal rates, elevated concentration of intermediate VOC species, or uncertainties in transport processes. Consequently, the simulated  $\text{pNO}_3^-$  formation from  $\text{N}_2\text{O}_5$  uptake in this study could be regarded as a lower limit. The simulated OH concentrations agreed well with parameterized method suggested by Ehhalt and Rohrer (**Figure S4**,  $R^2 = 0.86$ ) (Ehhalt and Rohrer, 2000). Based on model simulation and precursor observations, we quantified  $\text{pNO}_3^-$  formation rates through both  $\text{OH} + \text{NO}_2$  and  $\text{N}_2\text{O}_5$  uptake pathways by model integral.



### 2.3 Identification of influencing factors for $\text{pNO}_3^-$ Formation via $\text{N}_2\text{O}_5$ Uptake.

Extreme gradient boosting (XGBoost), a machine learning technique, has been widely applied in atmospheric chemistry research (Gui et al., 2020; Wang et al., 2023b; Requia et al., 2020). Here, we built a XGBoost model to reproduce the  $\text{pNO}_3^-$  formation rate via  $\text{N}_2\text{O}_5$  uptake with selected variables. The model was built using the “xgboost” library (<https://github.com/dmlc/xgboost/tree/master>) in a python environment. Explanatory variables included meteorological parameters (BLH, T, and RH), nocturnal atmospheric oxidation capacity  $\text{P}(\text{NO}_3)$  calculated by  $k_{\text{NO}_2+\text{O}_3}[\text{NO}_2][\text{O}_3]$ , TVOCs, the logarithm of the ratio of  $\text{NO}_2$  to  $\text{O}_3$  ( $\log([\text{NO}_2]/[\text{O}_3])$ ), NO, and heterogeneous uptake parameters ( $\phi\text{ClNO}_2$  and  $k_{\text{N}_2\text{O}_5}$ ). Only nighttime (18:00 – 06:00 the next day) data were considered to identify key drivers of  $\text{pNO}_3^-$  formation via  $\text{N}_2\text{O}_5$  uptake. The hyperparameters of the XGBoost model were tuned by grid searching method and the established model was evaluated using  $R^2$ , Mean Absolute Error (MAE) and Root Mean Square Error (RMSE). By incorporating SHAP interpretation, the XGBoost-SHAP method could quantify factor contributions through SHAP values, where absolute SHAP values denote the relative importance. Detailed description and setup of the XGBoost-SHAP method can be found in **Text S6** and our previous study (Lin et al., 2024).

### 2.4 Emission Scenario Modelling.

Using the aforementioned multiphase chemical box model, we investigated changes in formation rates of  $\text{pNO}_3^-$  ( $\text{PNO}_3^-$ ) and  $\text{O}_3$  ( $\text{PO}_3$ ) under different VOCs and  $\text{NO}_x$  emission scenarios. The base model simulation was performed using mean diurnal values from the winter 2022 observations. A series of emission scenarios were tested by scaling normalized VOCs and  $\text{NO}_x$  concentrations from 0 to 2 times baseline levels to examine their impacts on  $\text{PNO}_3^-$  and  $\text{PO}_3$ . Prior to each scenario simulation, 3-day spin-up was set to stabilize intermediate species concentrations. Isopleth diagrams of simulated  $\text{PNO}_3^-$  and  $\text{PO}_3$  were obtained from the base scenario and 120 emission change scenarios. In addition, response strength (RS) was calculated using **eq 2** as an indicator of emission sensitivity.

$$\text{PO}_3 = k_1[\text{HO}_2][\text{NO}] + \sum k_{2i}[\text{RO}_2][\text{NO}] \quad (1)$$

Where,  $k_i$  is the corresponding chemical reaction rate constants.

$$\text{RS} = \frac{X_i - X_{\text{base}}}{V_i - V_{\text{base}}} \quad (2)$$



Where,  $X_i$  and  $X_{\text{base}}$  are the mean formation rates of dependent variables e.g.  $\text{PNO}_3^-$ ,  $\text{PO}_3$  in scenario  $i$  and base simulations, respectively.  $V_i$  and  $V_{\text{base}}$  are the emission rates for the scenario  $i$  and base simulations, respectively. Notably, the emission rates ranged from 0 to 2 times baseline levels, with the base simulation emission rate normalized to 1.

### 3 Results and Discussion

#### 3.1 Overview of Observations.

The mean diurnal patterns of  $\text{pNO}_3^-$ , gaseous pollutants and relevant meteorological parameters are shown in **Figure 1**. During the entire observation period, mean concentrations of  $\text{NO}_2$ ,  $\text{O}_3$ , total VOCs, and  $\text{PM}_{2.5}$  were 10.9 ppb, 27.3 ppb, 18.2 ppb, and  $14.3 \mu\text{g m}^{-3}$ , respectively, lower than those observed in most of China's key cities (refer to **Table S1**). Despite the low  $\text{NO}_x$  levels,  $\text{pNO}_3^-$  contributed 29.5% to  $\text{PM}_{2.5}$  mass concentration, which was higher than proportions reported in Beijing urban area (24.7%) (Ma et al., 2023), Guangdong (24.0%) (Yun et al., 2018), and Nanjing (24%–27%) (Huang et al., 2020). This discrepancy suggests efficient conversion from  $\text{NO}_2$  to  $\text{pNO}_3^-$  in the study area. In addition, the proportion of  $\text{pNO}_3^-$  increased with rising  $\text{PM}_{2.5}$  concentration (**Figure S6**), indicating its importance to particulate pollution. This is consistent with the phenomenon widespread in urban areas of China where  $\text{pNO}_3^-$  became dominant in inorganic aerosols despite  $\text{NO}_x$  reduction, underscoring the need for efficient  $\text{pNO}_3^-$  control strategies (Zhai et al., 2021; Zhao et al., 2020; Zhang et al., 2022).

The diurnal pattern of  $\text{pNO}_3^-$  exhibited a bimodal characteristic, with peaks occurring at 4:00 and 15:00 LT, respectively. The daytime peak (07:00–17:00) was accompanied by low concentrations of  $\text{NO}_x$  and high levels of  $\text{O}_3$  and  $\text{JNO}_2$ , indicating that active photochemical conditions promoted daytime  $\text{pNO}_3^-$  formation. During the nighttime (18:00–06:00 the next day),  $\text{pNO}_3^-$  concentrations increased together with  $\text{NO}_2$ ,  $\text{N}_2\text{O}_5$  and  $\text{ClNO}_2$  from 18:00 onward and remained elevated until early morning. This nighttime accumulation can be attributed to two factors. First, lower temperature, shallower boundary layer height, and reduced wind speed at night favored the accumulation of  $\text{pNO}_3^-$  and related nitrogen-containing species. Second, higher RH and  $\text{PM}_{2.5}$  concentrations at night enhanced aerosol water content and surface area, providing favorable conditions for heterogeneous hydrolysis of  $\text{N}_2\text{O}_5$  to form  $\text{pNO}_3^-$ . The mean concentration of  $\text{N}_2\text{O}_5$  was  $0.19 \pm 0.26$  ppb (peaking at 2.52 ppb), which is relatively higher than values reported for China's megacities (Chen et al., 2020; Wang et al., 2017; Tham et al., 2018; Wang et al., 2022a; Liu et al., 2025; Li et al., 2023). Moreover, the observed elevation in nighttime  $\text{ClNO}_2$ ,



primarily produce via the reaction of  $\text{N}_2\text{O}_5$  with Cl-containing particles, strongly supports the presence of active heterogeneous processes of  $\text{N}_2\text{O}_5$ . Collectively, these findings imply a likely significant contribution of  $\text{N}_2\text{O}_5$  uptake to  $\text{pNO}_3^-$  formation during the nighttime.

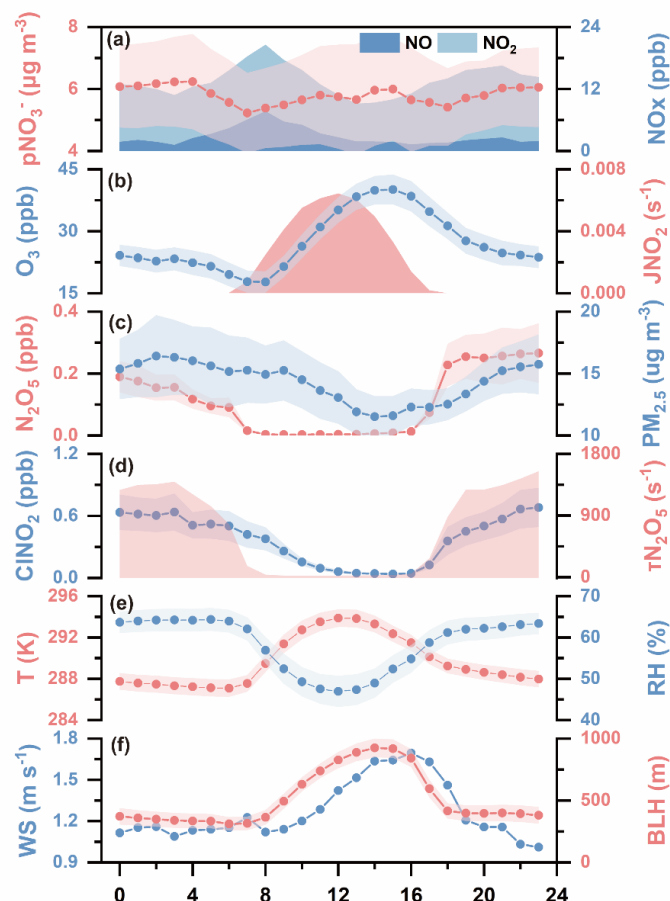


**Figure 1.** Diurnal variations of key parameters during the winter of 2022. The concentrations of  $\text{pNO}_3^-$ ,  $\text{NO}_x$ ,  $\text{O}_3$ ,  $\text{N}_2\text{O}_5$ ,  $\text{PM}_{2.5}$  and  $\text{ClNO}_2$ . The levels of the photolysis frequencies of  $\text{NO}_2$  ( $\text{JNO}_2$ ), ambient temperature ( $T$ ), relative humidity ( $\text{RH}$ ), the lifetime of  $\text{N}_2\text{O}_5$  ( $\tau\text{N}_2\text{O}_5$ ), wind speed ( $\text{WS}$ ) and the boundary layer height ( $\text{BLH}$ ). Shaded areas of  $\text{pNO}_3^-$ ,  $\text{O}_3$ ,  $\text{N}_2\text{O}_5$ ,  $\text{PM}_{2.5}$ ,  $\text{ClNO}_2$ ,  $T$ ,  $\text{RH}$  and  $\text{BLH}$  represent 95% confidence intervals.

### 3.2 High contribution of $\text{N}_2\text{O}_5$ uptake to $\text{pNO}_3^-$ formation in $\text{NO}_2$ -limited conditions.

In view of the observed importance of daytime and nighttime  $\text{pNO}_3^-$  formation, we further employed an observation-constrained model to quantify the potential formation pathways, including the gas-phase reaction of  $\text{OH} + \text{NO}_2$  and heterogeneous  $\text{N}_2\text{O}_5$  uptake. This model incorporated heterogeneous chemical mechanisms, with key heterogeneous parameters (e.g.  $k\text{N}_2\text{O}_5$  and  $\phi\text{ClNO}_2$ ) obtained through simulation



(See Methods for details). As shown in **Figure S7**, the simulated  $\text{kN}_2\text{O}_5$  and  $\phi\text{ClNO}_2$  exhibited good agreement with the classical steady-state method ( $R^2 = 0.76$  and  $0.73$ , respectively), demonstrating the model's capability to characterize heterogeneous uptake processes and thereby effectively evaluate  $\text{pNO}_3^-$  formation processes.

As illustrated in **Figure 2a**, the diurnal pattern of  $\text{pNO}_3^-$  formation rates exhibited a classical characteristic, with daytime dominated by gas-phase oxidation and nighttime dominated by  $\text{N}_2\text{O}_5$  uptake. Specifically, the daytime  $\text{OH} + \text{NO}_2$  reaction had a mean  $\text{pNO}_3^-$  formation rate of  $1.62 \mu\text{g m}^{-3} \text{h}^{-1}$ , while the nighttime  $\text{N}_2\text{O}_5$  uptake pathway showed a formation rate of  $1.18 \mu\text{g m}^{-3} \text{h}^{-1}$  (**Figure 2b-c**). For the whole day,  $\text{N}_2\text{O}_5$  uptake contributed an average of 51.2% to  $\text{pNO}_3^-$  formation, which was comparable to the contribution of the  $\text{OH} + \text{NO}_2$  pathway (**Figure 2d**). To exclude year-specific effects, we further analyzed  $\text{pNO}_3^-$  formation during the winters from 2019 to 2023. The results revealed that the  $\text{pNO}_3^-$  formation rates via  $\text{N}_2\text{O}_5$  uptake ( $0.75 - 1.40 \mu\text{g m}^{-3} \text{h}^{-1}$ ) were comparable to those from the  $\text{OH} + \text{NO}_2$  reaction ( $0.88 - 1.66 \mu\text{g m}^{-3} \text{h}^{-1}$ ; **Figure 3a**), with the  $\text{N}_2\text{O}_5$  uptake pathway consistently accounting for approximately half of the total  $\text{pNO}_3^-$  formation in the study area (**Figure 3b**). Such a high contribution of  $\text{N}_2\text{O}_5$  uptake to  $\text{pNO}_3^-$  is generally uncommon in urban areas. A study in urban Beijing showed that during non-polluted periods,  $\text{N}_2\text{O}_5$  uptake contributed only 18.9% to nitrate formation rates (Ma et al., 2023). Similarly, the contributions of  $\text{N}_2\text{O}_5$  uptake were 10% – 38% and 4% in urban areas of the YRD (Sun et al., 2022; Zhai et al., 2023; Zhang et al., 2023b) and PRD regions (Yang et al., 2022), respectively.

Previous studies have found that nocturnal  $\text{pNO}_3^-$  formation via  $\text{N}_2\text{O}_5$  uptake strongly depends on the ratio of  $\text{NO}_2$  to  $\text{O}_3$  (Ma et al., 2023). This process is suppressed in the  $\text{O}_3$ -limited regime ( $\text{NO}_2/\text{O}_3 > 2$ ) but enhanced in the  $\text{NO}_2$ -limited regime ( $\text{NO}_2/\text{O}_3 \leq 1$ ). The COVID-19 lockdown period was a typical example of this ratio dependence (Yan et al., 2023). In regions like Beijing, substantial reductions in  $\text{NO}_x$  emissions caused a shift in nocturnal  $\text{pNO}_3^-$  formation from the  $\text{O}_3$ -limited to the  $\text{NO}_2$ -limited regime. This shift resulted in elevated nighttime  $\text{O}_3$  levels and a weakened  $\text{NO}$  titration effect, collectively promoting  $\text{N}_2\text{O}_5$  formation and subsequent  $\text{pNO}_3^-$  formation. The sensitivity of  $\text{pNO}_3^-$  formation via  $\text{N}_2\text{O}_5$  uptake to  $\text{NO}_2$  and  $\text{O}_3$  during the campaign is presented in **Figure 3c-d**. The observed mean values of  $\text{NO}_2/\text{O}_3$  (0.40) and the probability distributions of  $\text{NO}_2/\text{O}_3$  ratios both indicate that  $\text{N}_2\text{O}_5$  uptake was in the  $\text{NO}_2$ -limited regime. Based on  $\text{NO}_2$  and  $\text{O}_3$  observational data during 2015–2021 from the China National Environmental Monitoring Centre (Ma et al., 2023), most key urban regions in China (e.g., the NCP, YRD, and Beijing) were found to lie in the  $\text{O}_3$ -limited or transition regimes ( $1 < \text{NO}_2/\text{O}_3 \leq 2$ ),



whereas nocturnal  $\text{pNO}_3^-$  formation in southeastern China was distinctly in  $\text{NO}_2$ -limited regime. These results confirm that the dominant  $\text{pNO}_3^-$  formation mechanisms in our study area significantly differs from those in most urban areas of China, which might be attributed to the dependence of  $\text{N}_2\text{O}_5$  uptake on precursor  $\text{NO}_2$  and  $\text{O}_3$ . In addition, the dominance of  $\text{N}_2\text{O}_5$  uptake in  $\text{pNO}_3^-$  formation also occurred during haze pollution periods (Zhai et al., 2023; Wang et al., 2017), where increased aerosol surface area under high particulate loadings created favorable conditions for  $\text{N}_2\text{O}_5$  heterogeneous reactions. Therefore, to evaluate the role of precursors, we conducted a comprehensive analysis of the factors driving  $\text{pNO}_3^-$  formation via  $\text{N}_2\text{O}_5$  uptake.

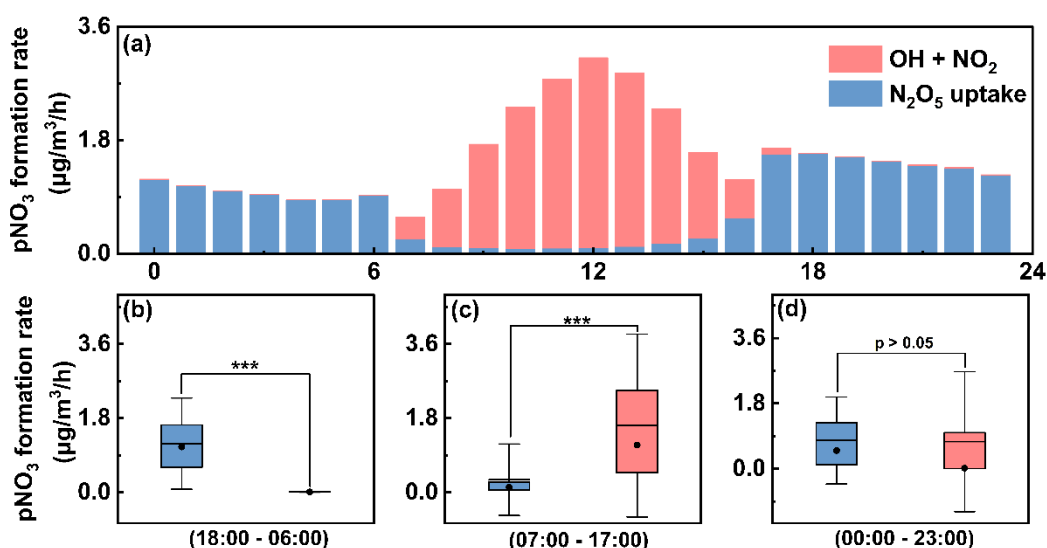


**Figure 2.** Simulated rates of key  $\text{pNO}_3^-$  formation pathways obtained from the chemical box model incorporating heterogeneous parameters. Diurnal formation rates of  $\text{pNO}_3^-$  via the  $\text{OH} + \text{NO}_2$  and  $\text{N}_2\text{O}_5$  uptake pathways (a) and comparison of the two pathways during the nighttime (b), daytime (c), and the whole day (d). Note that the results in panel (a) represent the mean simulated formation rates over the entire observation period. The box shows the 25th–75th percentiles with whiskers representing the 5th–95th percentiles. The black line and dot inside the box represent the mean and median values, respectively. Statistical significance was determined using pair-sample  $t$ -tests with \*\*\* indicating  $p < 0.001$ .



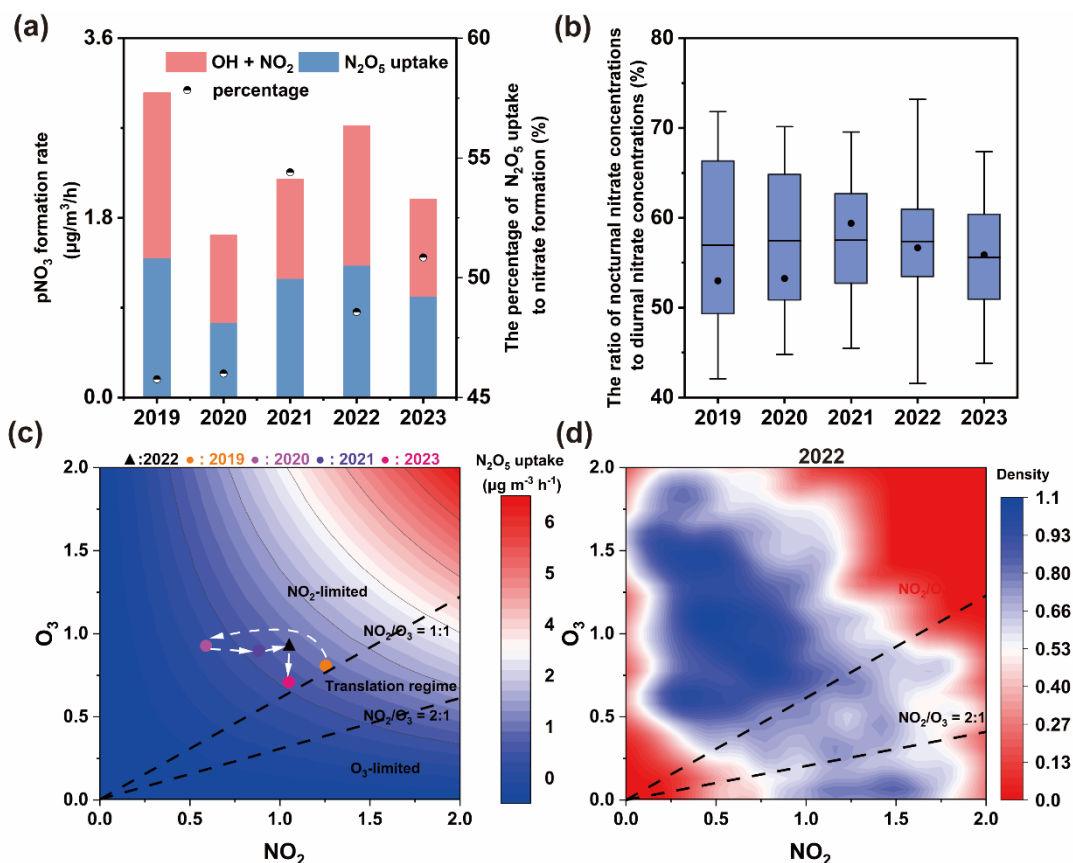


**Figure 3.** Inter-annual patterns of key  $\text{pNO}_3^-$  formation pathways in urban Xiamen. The average  $\text{pNO}_3^-$  formation rate from  $\text{OH} + \text{NO}_2$  and  $\text{N}_2\text{O}_5$  uptake (a), and the average ratio of the sum of nocturnal  $\text{pNO}_3^-$  concentrations to the sum of all-day  $\text{pNO}_3^-$  concentration (b) in different winters from 2019 to 2023 based on the measured  $\text{pNO}_3^-$  in  $\text{PM}_{2.5}$ . The sensitivity of nocturnal  $\text{pNO}_3^-$  formation via  $\text{N}_2\text{O}_5$  uptake to  $\text{NO}_2$  and  $\text{O}_3$  from 2019 to 2023 (c). And probability distribution of observed  $\text{NO}_2/\text{O}_3$  at nighttime in winter 2022 (d). The observed periods of different winters from 2019 to 2023 are summarized in Table S3. In panel (b), the black line and the solid circle in the boxplot represent the mean and median value, respectively. In panel (c), the black triangle indicates the base case of winter 2022, solid circles in different colors represent the average  $\text{NO}_2$  to  $\text{O}_3$  ratios in different years, and the predicted average formation rate of  $\text{N}_2\text{O}_5$  uptake as the normalized emissions (average concentrations of  $\text{O}_3$  and  $\text{NO}_2$ ) varied between 0 to 2.

### 3.3 Driving Factors of $\text{pNO}_3^-$ Formation via Nocturnal $\text{N}_2\text{O}_5$ Uptake.

The  $\text{N}_2\text{O}_5$  uptake rate is influenced by multiple factors including precursor levels, meteorological parameters, and heterogeneous reaction conditions (Ma et al., 2023; Chen et al., 2020; Chen et al., 2024).



A machine learning method integrating these factors was employed to identify the key drivers of  $\text{pNO}_3^-$  formation via  $\text{N}_2\text{O}_5$  uptake. The relative importance of each factor was evaluated by absolute SHAP values (**Figure 4a**), and their impacts were elucidated by examining the relationships between individual factors and their corresponding SHAP values (**Figure 4b-e** and **Figure S8**). Results showed that the nocturnal  $\text{NO}_3$  formation rate ( $\text{P}(\text{NO}_3)$ ), an integrated indicator of nocturnal atmospheric oxidation capacity (Wang et al., 2021), was the most important factor. The steep slope of the positive correlation between  $\text{P}(\text{NO}_3)$  and SHAP values indicated that  $\text{P}(\text{NO}_3)$  strongly enhances  $\text{pNO}_3^-$  formation via  $\text{N}_2\text{O}_5$  uptake.  $\text{P}(\text{NO}_3)$  is primarily formed through the reaction between  $\text{NO}_2$  and  $\text{O}_3$  ( $\text{P}(\text{NO}_3) = k_{\text{NO}_2+\text{O}_3}[\text{NO}_2][\text{O}_3]$ ), suggesting that  $\text{NO}_2$  and  $\text{O}_3$  mainly influenced  $\text{pNO}_3^-$  formation via  $\text{N}_2\text{O}_5$  by modulating  $\text{NO}_3$  radical formation. Notably, the factor  $\log\text{NO}_2/\text{O}_3$  had relatively low importance, indicating concentrations of precursors were more important than  $\text{NO}_2/\text{O}_3$  ratio in determining  $\text{pNO}_3^-$  formation via  $\text{N}_2\text{O}_5$  uptake under extremely  $\text{NO}_2$ -limited condition (mean  $\text{NO}_2/\text{O}_3$  was 0.40). Furthermore, as shown in **Figure S8b**,  $\log\text{NO}_2/\text{O}_3$  and its SHAP value show a positive correlation when  $\log\text{NO}_2/\text{O}_3$  is less than 0. This indicates that under  $\text{NO}_2$ -limited conditions ( $\log\text{NO}_2/\text{O}_3 < 0$ , i.e.,  $\text{NO}_2/\text{O}_3 < 1$ ),  $\text{pNO}_3^-$  formation via  $\text{N}_2\text{O}_5$  uptake was driven by the elevated  $\text{NO}_2$ .

Compared with  $\text{P}(\text{NO}_3)$ , other factors exhibited weaker effects on  $\text{pNO}_3^-$  formation rate via  $\text{N}_2\text{O}_5$  uptake.  $\phi\text{ClNO}_2$  emerged as the second most important factor and showed a negative correlation with SHAP values (**Figure 4c**), illustrating that  $\text{ClNO}_2$  formation inhibited  $\text{pNO}_3^-$  formation. This inhibitory effect could be attributed to high concentrations of Cl-containing particles ( $0.94 \pm 1.11 \mu\text{g m}^{-3}$ ) in the study area. Chloride-containing aerosols promote  $\text{N}_2\text{O}_5$  uptake to produce more  $\text{ClNO}_2$  (as evidenced by the positive correlation between  $\phi\text{ClNO}_2$  and chloride ions, **Figure S9**), while simultaneously reducing  $\text{pNO}_3^-$  formation (R5). Additionally, the nighttime produced  $\text{ClNO}_2$  can undergo photolysis in following day to release Cl radicals, which further promote  $\text{O}_3$  formation. This indirect effect must be considered when formulating control measures for particulate matter pollution. Interestingly, as shown in **Table S4** (Tham et al., 2016; Wang et al., 2018; Yun et al., 2018; Morgan et al., 2015), although the simulated  $k_{\text{N}_2\text{O}_5}$  ( $7.64 \times 10^{-3} \pm 6.12 \times 10^{-3} \text{ s}^{-1}$ ) was higher than values reported in Beijing ( $8.1 \times 10^{-4} - 1.42 \times 10^{-3} \text{ s}^{-1}$ ), Guangdong ( $3.78 \times 10^{-3} - 9 \times 10^{-3} \text{ s}^{-1}$ ), and UK ( $9.3 \times 10^{-5} - 10^{-3} \text{ s}^{-1}$ ),  $k_{\text{N}_2\text{O}_5}$  exerted only a weak positive effect on  $\text{N}_2\text{O}_5$  uptake (**Figure 4d**). The large difference existing in the importance of  $\text{P}(\text{NO}_3)$  and  $k_{\text{N}_2\text{O}_5}$  indicated that the  $\text{pNO}_3^-$  formation rate via  $\text{N}_2\text{O}_5$  uptake process was more limited by precursor levels rather than heterogeneous uptake conditions. Similar phenomenon was also found in winter in urban



Beijing and Northern Utah mountain basins (Mcduffie et al., 2019; Chen et al., 2020). The total concentrations of the observed VOCs (TVOCs) showed a weak negative correlation with  $\text{N}_2\text{O}_5$  uptake (Figure 4e). Similar to existing research (Hu et al., 2023), specific VOC species, such as styrene, 2-butene, and isoprene, can readily consume  $\text{NO}_3$  radicals (Figure S10), thereby inhibiting  $\text{N}_2\text{O}_5$  formation. However, the loss of  $\text{N}_2\text{O}_5$  through the reaction between VOCs and  $\text{NO}_3$  was relatively limited compared to its direct uptake, as determined by our calculations (Text S4), which supported the SHAP analysis.

Moreover, we found that the effects of  $\phi\text{ClNO}_2$ ,  $k\text{N}_2\text{O}_5$ , and TVOCs on  $\text{pNO}_3^-$  formation via  $\text{N}_2\text{O}_5$  uptake were subject to  $\text{P}(\text{NO}_3)$  levels (Figure 5a-5c). Specifically, the negative effect of  $\phi\text{ClNO}_2$  and the positive effect of  $k\text{N}_2\text{O}_5$  on  $\text{pNO}_3^-$  formation via  $\text{N}_2\text{O}_5$  uptake became statistically significant when  $\text{P}(\text{NO}_3)$  exceeded approximately  $1.0 \text{ ppb h}^{-1}$  and  $0.5 \text{ ppb h}^{-1}$ , respectively. The negative correlation slope of TVOCs versus  $\text{pNO}_3^-$  formation via  $\text{N}_2\text{O}_5$  uptake intensified with increasing  $\text{P}(\text{NO}_3)$  levels, indicating that the  $\text{N}_2\text{O}_5$  removal effect was enhanced through VOC-induced  $\text{NO}_3$  depletion. These findings highlight the critical role of precursor  $\text{NO}_2$  and  $\text{O}_3$  in nocturnal  $\text{pNO}_3^-$  formation, demonstrating that these precursors mainly affect this pathway by modulating  $\text{NO}_3$  radical formation.



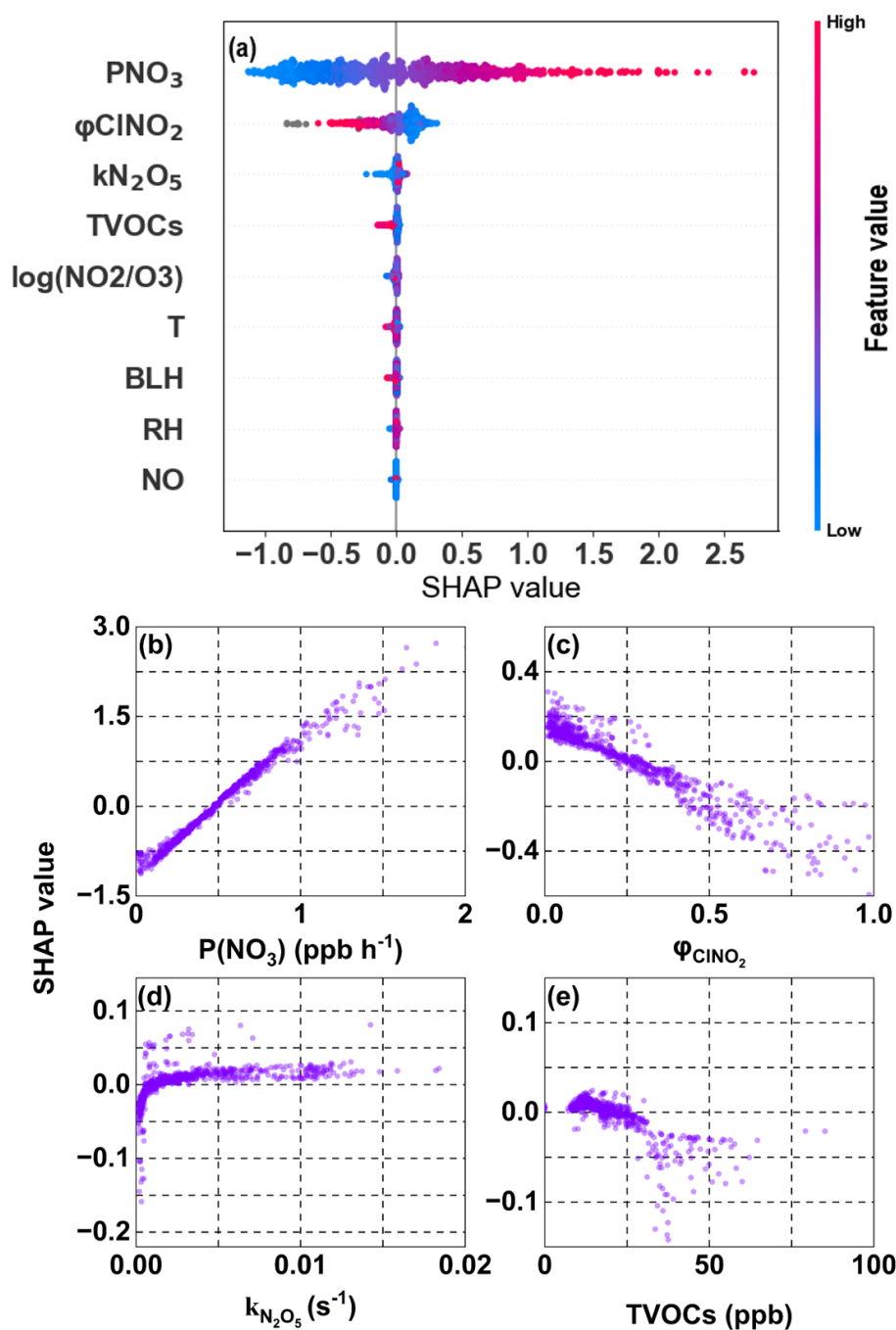


**Figure 4.** Feature importance (a) and the effects of key factors on  $\text{pNO}_3^-$  formation via  $\text{N}_2\text{O}_5$  uptake (b-e) obtained by the XGBoost-SHAP method. The relationships between SHAP values and major features:  $\text{P}(\text{NO}_3)$  (b),  $\phi\text{CINO}_2$ (c),  $\text{kN}_2\text{O}_5$ (d), and TVOCs (e). Feature importance ranking (a) is determined by mean absolute SHAP values (descending order, top to bottom). Relationships between SHAP values and other factors are shown in Figure S8.



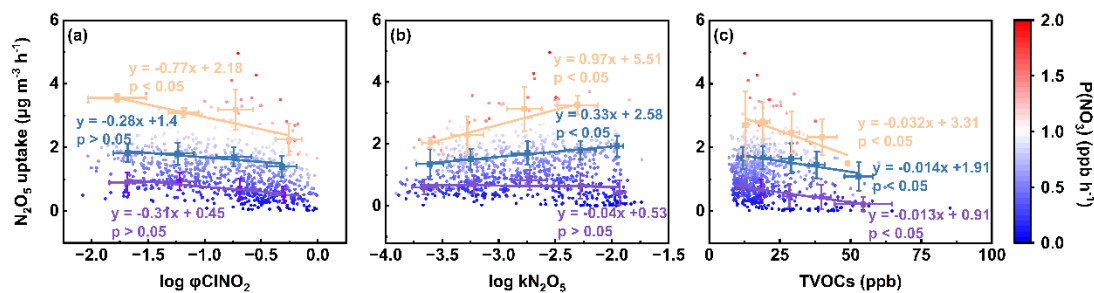


**Figure 5.** Relationships between  $pNO_3^-$  formation via  $N_2O_5$  uptake and  $\phi ClNO_2$  (a),  $kN_2O_5$  (b), and TVOCs (c) colored by  $P(NO_3)$ . Linear fit curves in purple, blue and orange represent the fitting results for  $P(NO_3)$  in the ranges of 0–0.5 ppb  $h^{-1}$ , 0.5–1.0 ppb  $h^{-1}$  and  $> 1.0$  ppb  $h^{-1}$ , respectively.

### 3.4 Optimal Mitigation Strategies of $pNO_3^-$ under $NO_2$ -limited conditions.

The above results revealed that  $pNO_3^-$  formation through both the daytime  $OH + NO_2$  reaction and nocturnal heterogeneous  $N_2O_5$  uptake was closely linked to VOCs- $NO_x$ - $O_3$  chemistry (Yang et al., 2022). Using a multiphase box model, we systematically examined the responses of both  $pNO_3^-$  and  $O_3$  to varying  $NO_x$  and VOC emission scenarios. **Figure 6a** shows  $pNO_3^-$  formation located in the transition regime of VOCs and  $NO_x$ . The formation rate of  $pNO_3^-$  ( $PNO_3^-$ ) decreased with the reductions of VOCs and  $NO_x$ , and this trend became more pronounced under aggressive  $NO_x$  reduction scenarios (**Figure 6c-d**). **Figure S11a-b** reveal that the mean response strength (RS, as defined in Methods) of  $PNO_3^-$  to  $NO_x$  was 0.75, higher than that for VOCs ( $RS = 0.29$ ), suggesting that  $NO_x$  reduction had a greater potential for  $pNO_3^-$  mitigation compared to VOCs control. However,  $NO_x$  and VOCs reductions exerted different impacts on  $O_3$  formation rate ( $PO_3$ ). In our study area,  $PO_3$  located in the VOC-limited regime (**Figure 6b**). We found that  $PO_3$  declined with VOCs reduction but increased with  $NO_x$  reduction until  $NO_x$  dropped below 20% of the base (**Figure 5c-d**). Moreover, detailed results distinguishing daytime and nighttime major formation pathways of  $pNO_3^-$  are presented in **Figure 6e-f** and **Fig. S11c-d**. For VOC reduction scenarios, both the  $OH + NO_2$  reaction and  $N_2O_5$  uptake pathways showed declining nitrate formation rates, with comparable RS of 0.11 and 0.18, respectively. This occurs because reduced VOCs concentrations decrease  $OH$  radical and  $O_3$  concentrations, thereby suppressing  $pNO_3^-$  formation via both pathways. In contrast,  $NO_x$  reduction yielded more complex behavior. The  $OH + NO_2$  reaction rates remained nearly constant until  $NO_x$  dropped to 60% of the base. This stability arises because  $NO_x$  reduction diminishes the  $NO$  titration effect on  $O_3$ , thereby increasing  $OH$  radicals through  $O_3$  photolysis.



The competing effects of NO<sub>x</sub> reduction and OH enhancement led to an initial plateau in the OH + NO<sub>2</sub> reaction rate before its eventual decline. Differently, the N<sub>2</sub>O<sub>5</sub> uptake rate decreased consistently and significantly with NO<sub>x</sub> abatement, exhibiting a high mean RS value of 0.61. This phenomenon was closely associated with the NO<sub>2</sub>-limited regime of N<sub>2</sub>O<sub>5</sub> uptake in the study area. As shown in **Figure S12**, the variation trends of PNO<sub>3</sub><sup>-</sup>, P(O<sub>3</sub>), OH + NO<sub>2</sub>, and N<sub>2</sub>O<sub>5</sub> uptake were consistent across all VOCs/NO<sub>x</sub> combinations, indicating that the results robustly reflect the response mechanisms to precursor emission changes.

As mentioned above, while VOCs reduction proved effective in mitigating both pNO<sub>3</sub><sup>-</sup> and O<sub>3</sub>, its effectiveness in reducing pNO<sub>3</sub><sup>-</sup> remained limited compared to NO<sub>x</sub> reduction. However, the effectiveness of NO<sub>x</sub> reduction exhibited significant regional and temporal variations. In China's megacities, including PRD, YRD, and BTH regions, pNO<sub>3</sub><sup>-</sup> initially increased and then decreased in response to the reduction of NO<sub>x</sub> emissions (Li et al., 2021; Zhang et al., 2023b; Yang et al., 2022). Under high-NO<sub>x</sub> conditions, mild NO<sub>x</sub> reduction would raise daytime OH and O<sub>3</sub> concentrations (Zhang et al., 2023b), rendering OH (rather than NO<sub>x</sub>) the limiting factor for the OH + NO<sub>2</sub> reaction, which consequently enhanced daytime pNO<sub>3</sub><sup>-</sup> formation. Additionally, as the season most susceptible to PM pollution, wintertime N<sub>2</sub>O<sub>5</sub> formation in these regions was in an O<sub>3</sub>-limited or transition regime (Ma et al., 2023), wherein the elevated daytime O<sub>3</sub> significantly enhanced NO<sub>3</sub> radical generation, thereby promoting nocturnal N<sub>2</sub>O<sub>5</sub> uptake and subsequent pNO<sub>3</sub><sup>-</sup> formation. Conversely, in NO<sub>2</sub>-limited regions (e.g., southeastern China), NO<sub>x</sub> reduction showed limited impact on daytime pNO<sub>3</sub><sup>-</sup> formation via the OH + NO<sub>2</sub> pathway but effectively suppressed nighttime pNO<sub>3</sub><sup>-</sup> formation via N<sub>2</sub>O<sub>5</sub> uptake. This approach concurrently reduced ClNO<sub>2</sub> formation from N<sub>2</sub>O<sub>5</sub> heterogeneous processes, consequently diminishing next-day Cl radical generation and its positive feedback on O<sub>3</sub> formation. Considering NO<sub>x</sub> reduction during the daytime would cause O<sub>3</sub> formation and only a slight reduction in pNO<sub>3</sub><sup>-</sup>, it is preferable to regulate NO<sub>x</sub> at night (18:00–06:00 the next day). Our findings demonstrate that in regions with a NO<sub>2</sub>-limited for pNO<sub>3</sub><sup>-</sup> formation, targeted NO<sub>x</sub> reduction can synergistically decrease both pNO<sub>3</sub><sup>-</sup> and O<sub>3</sub> concentrations, highlighting the critical need to tailor mitigation strategies for different regions.



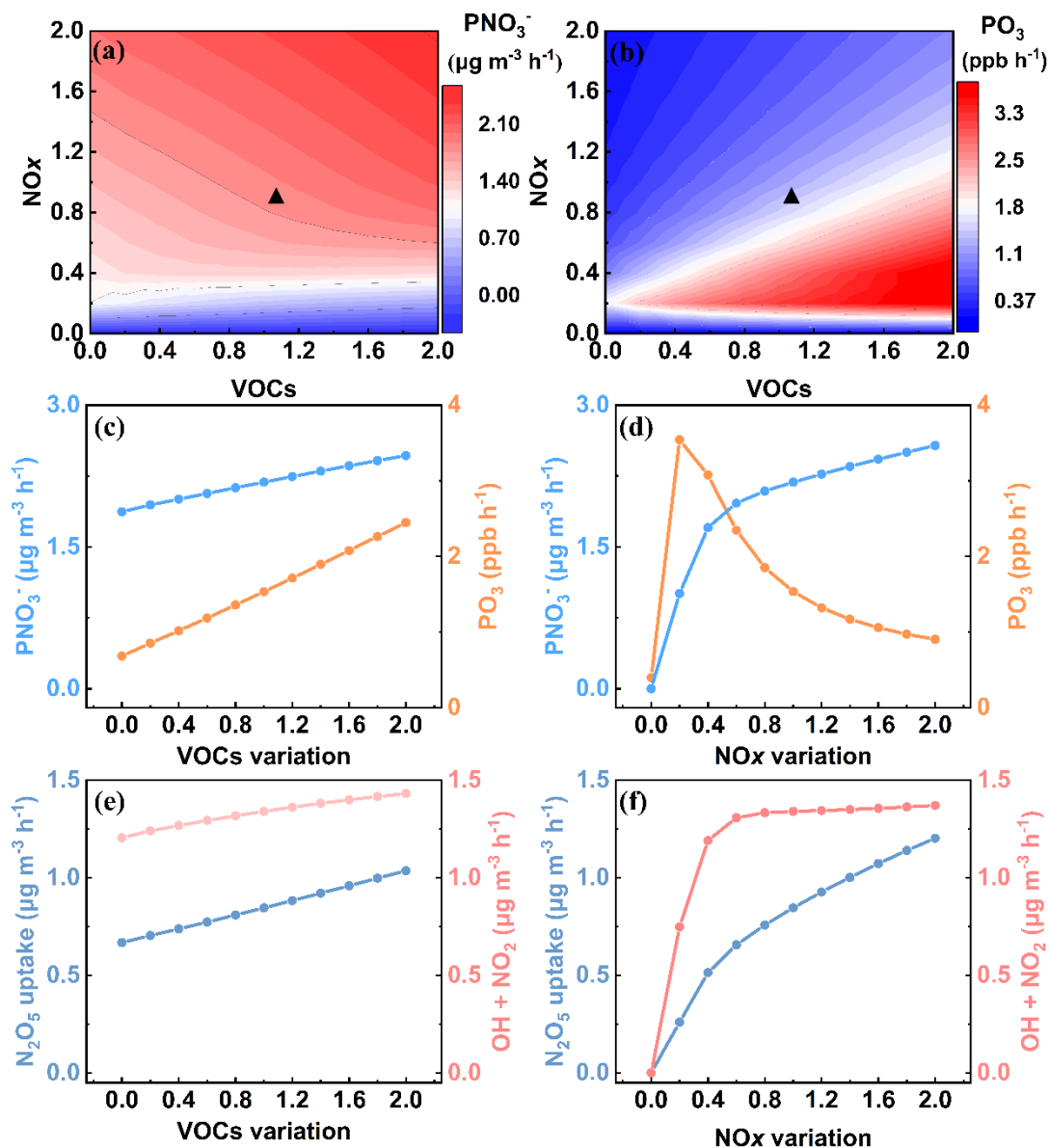


**Figure 6.** Results of multi-scenario simulations obtained from an observation-constrained box model. Isopleths of simulated  $\text{PNO}_3^-$  (a) and  $\text{PO}_3$  (b) with normalized VOCs and NOx. Simulated mean formation rates of  $\text{pNO}_3^-$  and  $\text{O}_3$  (c, d), as well as  $\text{pNO}_3^-$  formation rates via  $\text{N}_2\text{O}_5$  uptake and  $\text{OH} + \text{NO}_2$  (e, f) with normalized VOCs and NOx. The  $\text{PNO}_3^-$  and  $\text{PO}_3$  denote the formation rates of  $\text{pNO}_3^-$  and  $\text{O}_3$ , respectively. The simulated results are daily mean values, and the black triangle indicates the base case for winter 2022. In addition, the results in panel c-f were obtained by maintaining either NOx or VOCs at the base emission rate while varying the other.

## Conclusions and Implications

Our observations revealed a bimodal diurnal pattern of  $\text{pNO}_3^-$  in winter in urban Xiamen. The co-



occurrence of elevated nighttime  $\text{pNO}_3^-$  levels with increased  $\text{N}_2\text{O}_5$  implied a significant contribution of  $\text{N}_2\text{O}_5$  uptake to  $\text{pNO}_3^-$  formation. Quantitative model analysis showed that  $\text{N}_2\text{O}_5$  uptake contributed 51.2% of the total  $\text{pNO}_3^-$ , which was comparable to the  $\text{OH} + \text{NO}_2$  reaction. This high contribution of  $\text{N}_2\text{O}_5$  uptake to  $\text{pNO}_3^-$  is not commonly observed across Chinese cities. Comparative analysis among different cities suggests that this phenomenon is likely associated with  $\text{NO}_2$ -limited conditions for  $\text{N}_2\text{O}_5$  uptake in our study area. Machine learning results further demonstrated that  $\text{pNO}_3^-$  formation via  $\text{N}_2\text{O}_5$  uptake was driven by nocturnal atmospheric oxidation capacity ( $\text{PNO}_3$ ) rather than heterogeneous uptake conditions. The underlying mechanism is that the weakened  $\text{NO}_x$  titration effects lead to nighttime  $\text{O}_3$  accumulation, which promotes  $\text{NO}_3$  radical generation and consequently enhances  $\text{N}_2\text{O}_5$  and  $\text{pNO}_3^-$  formation. The joint response of  $\text{pNO}_3^-$  and  $\text{O}_3$  to various  $\text{NO}_x$  and VOCs emission scenarios indicated that  $\text{pNO}_3^-$  was more sensitive to  $\text{NO}_x$  reduction than to VOCs reduction. However, mild  $\text{NO}_x$  reduction showed limited effectiveness in reducing daytime  $\text{pNO}_3^-$  while simultaneously increasing  $\text{O}_3$  concentrations. Our findings suggest that  $\text{NO}_x$  reduction is more effective when implemented during nighttime, particularly in regions where  $\text{N}_2\text{O}_5$  formation is  $\text{NO}_2$ -limited. This approach can effectively control  $\text{pNO}_3^-$  formation by suppressing nocturnal  $\text{NO}_3$  radical generation and consequently inhibiting  $\text{N}_2\text{O}_5$  uptake, while simultaneously alleviate  $\text{O}_3$  pollution by reducing  $\text{ClNO}_2$  formation. With continuous  $\text{NO}_x$  and VOCs emission reductions and renewable energy adoption in China, urban areas are transitioning from  $\text{NO}_x$ -saturated to  $\text{NO}_x$ -limited conditions, potentially increasing the importance of the  $\text{N}_2\text{O}_5$  uptake pathway. In this context, comprehensive assessment of  $\text{NO}_x$  reduction impacts on urban  $\text{pNO}_3^-$  and  $\text{O}_3$  pollution, along with the development of region-specific mitigation strategies, becomes critically important.

#### **Data Availability**

The dataset for this paper can be accessed at <https://doi.org/10.6084/m9.figshare.29670629> (Lin et al., 2025).

#### **Code Availability**

Data analysis methods are available from the authors upon request.

#### **Acknowledgements**

This work was funded by the National Natural Science Foundation of China (U22A20578), the guiding



project of seizing the commanding heights of “self-purifying city” (IUE-CERAE-202402), the National Key Research and Development Program (2022YFC3700304), STS Plan Supporting Project of the Chinese Academy of Sciences in Fujian Province (2023T3013), and Xiamen Atmospheric Environment Observation and Research Station of Fujian Province.

#### Author Contribution

Z.L. contributed to the methodology, data curation, software, analysis and writing of the original draft. L.X. and J.C. contributed to the conceptualization, investigation, data curation, reviewing and editing the text, supervision, and funding acquisition. C.Y., X.J., K.Z., F.Z., G.C., L.L., C.Y., Y.C., and Z.C. provided useful advice and revised the manuscript.

#### Competing interests

The authors declare no competing interests.

#### References

- Atkinson, R. and Arey, J.: Atmospheric degradation of volatile organic compounds, Chemical Reviews. 103, 4605-4638, <https://doi.org/10.1021/cr0206420>, 2003.
- Brown, S. S. and Stutz, J.: Nighttime radical observations and chemistry, Chemical Society Reviews. 41, 6405-6447, <https://doi.org/10.1039/c2cs35181a>, 2012.
- Brown, S. S., Stark, H., and Ravishankara, A. R.: Applicability of the steady state approximation to the interpretation of atmospheric observations of NO<sub>3</sub> and N<sub>2</sub>O<sub>5</sub>: art. no. 4539, Journal of Geophysical Research-Atmospheres. 108, <https://doi.org/10.1029/2003jd003407>, 2003.
- Chen, X., Ma, W., Zheng, F. X., Wang, Z. C., Hua, C. J., Li, Y. R., Wu, J., Li, B. D., Jiang, J. K., Yan, C., Petäjä, T., Bianchi, F., Kerminen, V. M., Worsnop, D. R., Liu, Y. C., Xia, M., and Kulmala, M.: Identifying Driving Factors of Atmospheric N<sub>2</sub>O<sub>5</sub> with Machine Learning, Environmental Science & Technology. <https://doi.org/10.1021/acs.est.4c00651>, 2024.
- Chen, X. R., Wang, H. C., and Lu, K. D.: Interpretation of NO<sub>3</sub>-N<sub>2</sub>O<sub>5</sub> observation via steady state in high-aerosol air mass: the impact of equilibrium coefficient in ambient conditions, Atmospheric Chemistry and Physics. 22, 3525-3533, <https://doi.org/10.5194/acp-22-3525-2022>, 2022.
- Chen, X. R., Wang, H. C., Lu, K. D., Li, C. M., Zhai, T. Y., Tan, Z. F., Ma, X. F., Yang, X. P., Liu, Y. H., Chen, S. Y., Dong, H. B., Li, X., Wu, Z. J., Hu, M., Zeng, L. M., and Zhang, Y. H.: Field Determination of Nitrate Formation Pathway in Winter Beijing, Environmental Science & Technology. 54, 9243-9253, <https://doi.org/10.1021/acs.est.0c00972>, 2020.
- Cheng, C. L., Yang, S. X., Yuan, B., Pei, C. L., Zhou, Z. H., Mao, L. Y., Liu, S. L., Chen, D. Y., Cheng, X. Y., Li, M., Shao, M., and Zhou, Z.: The significant contribution of nitrate to a severe haze event in the winter of Guangzhou, China, Science of the Total Environment. 909, <https://doi.org/10.1016/j.scitotenv.2023.168582>, 2024.



Ehhalt, D. H. and Rohrer, F.: Dependence of the OH concentration on solar UV, *Journal of Geophysical Research-Atmospheres*. 105, 3565-3571, <https://doi.org/10.1029/1999jd901070>, 2000.

Fu, X. X., Wang, X. M., Liu, T. Y., He, Q. F., Zhang, Z., Zhang, Y. L., Song, W., Dai, Q. W., Chen, S., and Dong, F. Q.: Secondary inorganic aerosols and aerosol acidity at different PM<sub>2.5</sub> pollution levels during winter haze episodes in the Sichuan Basin, China, *Science of the Total Environment*. 918, <https://doi.org/10.1016/j.scitotenv.2024.170512>, 2024.

Gui, K., Che, H. Z., Zeng, Z. L., Wang, Y. Q., Zhai, S. X., Wang, Z. M., Luo, M., Zhang, L., Liao, T. T., Zhao, H. J., Li, L., Zheng, Y., and Zhang, X. Y.: Construction of a virtual PM<sub>2.5</sub> observation network in China based on high-density surface meteorological observations using the Extreme Gradient Boosting model, *Environment International*. 141, <https://doi.org/10.1016/j.envint.2020.105801>, 2020.

Hersbach, H., Bell, B., Berrisford, P., Hirahara, S., Horányi, A., Muñoz-Sabater, J., Nicolas, J., Peubey, C., Radu, R., Schepers, D., Simmons, A., Soci, C., Abdalla, S., Abellan, X., Balsamo, G., Bechtold, P., Biavati, G., Bidlot, J., Bonavita, M., De Chiara, G., Dahlgren, P., Dee, D., Diamantakis, M., Dragani, R., Flemming, J., Forbes, R., Fuentes, M., Geer, A., Haimberger, L., Healy, S., Hogan, R. J., Hólm, E., Janisková, M., Keeley, S., Laloyaux, P., Lopez, P., Lupu, C., Radnoti, G., de Rosnay, P., Rozum, I., Vamborg, F., Villaume, S., and Thépaut, J. N.: The ERA5 global reanalysis, *Quarterly Journal of the Royal Meteorological Society*. 146, 1999-2049, <https://doi.org/10.1002/qj.3803>, 2020.

Hu, H., Wang, H., Lu, K., Wang, J., Zheng, Z., Xu, X., Zhai, T., Chen, X., Lu, X., Fu, W., Li, X., Zeng, L., Hu, M., Zhang, Y., and Fan, S.: Variation and trend of nitrate radical reactivity towards volatile organic compounds in Beijing, China, *Atmos. Chem. Phys.*, 23, 8211-8223, <https://doi.org/10.5194/acp-23-8211-2023>, 2023.

Huang, X., Ding, A. J., Wang, Z. L., Ding, K., Gao, J., Chai, F. H., and Fu, C. B.: Amplified transboundary transport of haze by aerosol-boundary layer interaction in China, *Nature Geoscience*. 13, 428-+, <https://doi.org/10.1038/s41561-020-0583-4>, 2020.

Jenkin, M. E., Young, J. C., and Rickard, A. R.: The MCM v3.3.1 degradation scheme for isoprene, *Atmospheric Chemistry and Physics*. 15, 11433-11459, <https://doi.org/10.5194/acp-15-11433-2015>, 2015.

Lelieveld, J., Evans, J. S., Fnais, M., Giannadaki, D., and Pozzer, A.: The contribution of outdoor air pollution sources to premature mortality on a global scale, *Nature*. 525, 367-+, <https://doi.org/10.1038/nature15371>, 2015.

Li, F. B., Huang, D. D., Nie, W., Tham, Y. J., Lou, S. R., Li, Y. Y., Tian, L. H., Liu, Y. L., Zhou, M., Wang, H. C., Qiao, L. P., Wang, H. L., Wang, Z., Huang, C., and Li, Y. J.: Observation of nitrogen oxide-influenced chlorine chemistry and source analysis of Cl<sub>2</sub> in the Yangtze River Delta, China, *Atmospheric Environment*. 306, <https://doi.org/10.1016/j.atmosenv.2023.119829>, 2023.

Li, M. M., Zhang, Z. H., Yao, Q., Wang, T. J., Xie, M., Li, S., Zhuang, B. L., and Han, Y.: Nonlinear responses of particulate nitrate to NO<sub>x</sub> emission controls in the megalopolises of China, *Atmospheric Chemistry and Physics*. 21, 15135-15152, <https://doi.org/10.5194/acp-21-15135-2021>, 2021.

Lin, Z., Xu, L., Yang, C., Chen, G., Ji, X., Li, L., Zhang, K., Hong, Y., Li, M., Fan, X., Hu, B., Zhang, F., and Chen, J.: Trends of peroxyacetyl nitrate and its impact on ozone over 2018–2022 in urban atmosphere, *npj Climate and Atmospheric Science*. 7, 192, <https://doi.org/10.1038/s41612-024-00746-7>, 2024.

Liu, M. X., Huang, X., Song, Y., Tang, J., Cao, J. J., Zhang, X. Y., Zhang, Q., Wang, S. X., Xu, T. T., Kang, L., Cai, X. H., Zhang, H. S., Yang, F. M., Wang, H. B., Yu, J. Z., Lau, A. K. H., He, L. Y., Huang, X. F., Duan, L., Ding, A. J., Xue, L. K., Gao, J., Liu, B., and Zhu, T.: Ammonia emission control in China would mitigate haze pollution and nitrogen deposition, but worsen acid rain, *Proceedings of the National*



Academy of Sciences of the United States of America. 116, 7760-7765,  
<https://doi.org/10.1073/pnas.1814880116>, 2019.

Liu, T. T., Hong, Y. W., Li, M. R., Xu, L. L., Chen, J. S., Bian, Y. H., Yang, C., Dan, Y. B., Zhang, Y. N.,  
 Xue, L. K., Zhao, M., Huang, Z., and Wang, H.: Atmospheric oxidation capacity and ozone pollution  
 mechanism in a coastal city of southeastern China: analysis of a typical photochemical episode by an  
 observation-based model, *Atmospheric Chemistry and Physics*. 22, 2173-2190,  
<https://doi.org/10.5194/acp-22-2173-2022>, 2022.

Liu, Y., Wang, Y., Ma, P., Ma, Y., Pan, Y., Ma, W., Li, S., Liu, P., Liao, Z., Liu, Z., Chu, B., Ma, Q., Quan,  
 J., and He, H.: Formation of Nitrate in the Residual Layer of Beijing: Pathways Evaluation and  
 Contributions to the Ground Level, *Environmental Science & Technology*. 59, 9699-9708,  
<https://doi.org/10.1021/acs.est.5c02981>, 2025.

Ma, P. K., Quan, J. N., Dou, Y. J., Pan, Y. B., Liao, Z. H., Cheng, Z. G., Jia, X. C., Wang, Q. Q., Zhan, J.  
 L., Ma, W., Zheng, F. X., Wang, Y. Z., Zhang, Y. S., Hua, C. J., Yan, C., Kulmala, M., Liu, Y. A., Huang,  
 X., Yuan, B., Brown, S. S., and Liu, Y. C.: Regime-Dependence of Nocturnal Nitrate Formation via  $\text{N}_2\text{O}_5$   
 Hydrolysis and Its Implication for Mitigating Nitrate Pollution, *Geophysical Research Letters*. 50,  
<https://doi.org/10.1029/2023gl106183>, 2023.

Mao, J. Y., Yan, F. H., Zheng, L. M., You, Y. C., Wang, W. W., Jia, S. G., Liao, W. H., Wang, X. M., and  
 Chen, W. H.: Ozone control strategies for local formation- and regional transport-dominant scenarios in  
 a manufacturing city in southern China, *Science of the Total Environment*. 813,  
<https://doi.org/10.1016/j.scitotenv.2021.151883>, 2022.

McDuffie, E. E., Womack, C. C., Fibiger, D. L., Dube, W. P., Franchin, A., Middlebrook, A. M.,  
 Goldberger, L., Lee, B., Thornton, J. A., Moravek, A., Murphy, J. G., Baasandorj, M., and Brown, S. S.:  
 On the contribution of nocturnal heterogeneous reactive nitrogen chemistry to particulate matter  
 formation during wintertime pollution events in Northern Utah, *Atmospheric Chemistry and Physics*. 19,  
 9287-9308, <https://doi.org/10.5194/acp-19-9287-2019>, 2019.

McDuffie, E. E., Fibiger, D. L., Dubé, W. P., Hilfiker, F. L., Lee, B. H., Jaeglé, L., Guo, H. Y., Weber, R.  
 J., Reeves, J. M., Weinheimer, A. J., Schroder, J. C., Campuzano-Jost, P., Jimenez, J. L., Dibb, J. E.,  
 Veres, P., Ebben, C., Sparks, T. L., Wooldridge, P. J., Cohen, R. C., Campos, T., Hall, S. R., Ullmann, K.,  
 Roberts, J. M., Thornton, J. A., and Brown, S. S.:  $\text{ClNO}_2$  Yields From Aircraft Measurements During the  
 2015 WINTER Campaign and Critical Evaluation of the Current Parameterization, *Journal of*  
*Geophysical Research-Atmospheres*. 123, 12994-13015, <https://doi.org/10.1029/2018jd029358>, 2018a.

McDuffie, E. E., Fibiger, D. L., Dubé, W. P., Lopez-Hilfiker, F., Lee, B. H., Thornton, J. A., Shah, V.,  
 Jaeglé, L., Guo, H. Y., Weber, R. J., Reeves, J. M., Weinheimer, A. J., Schroder, J. C., Campuzano-Jost,  
 P., Jimenez, J. L., Dibb, J. E., Veres, P., Ebben, C., Sparks, T. L., Wooldridge, P. J., Cohen, R. C.,  
 Hornbrook, R. S., Apel, E. C., Campos, T., Hall, S. R., Ullmann, K., and Brown, S. S.: Heterogeneous  
 $\text{N}_2\text{O}_5$  Uptake During Winter: Aircraft Measurements During the 2015 WINTER Campaign and Critical  
 Evaluation of Current Parameterizations, *Journal of Geophysical Research-Atmospheres*. 123, 4345-  
 4372, <https://doi.org/10.1002/2018jd028336>, 2018b.

Morgan, W. T., Ouyang, B., Allan, J. D., Aruffo, E., Di Carlo, P., Kennedy, O. J., Lowe, D., Flynn, M. J.,  
 Rosenberg, P. D., Williams, P. I., Jones, R., McFiggans, G. B., and Coe, H.: Influence of aerosol chemical  
 composition on  $\text{N}_2\text{O}_5$  uptake: airborne regional measurements in northwestern Europe, *Atmospheric*  
*Chemistry and Physics*. 15, 973-990, <https://doi.org/10.5194/acp-15-973-2015>, 2015.

Niu, Y. B., Zhu, B., He, L. Y., Wang, Z., Lin, X. Y., Tang, M. X., and Huang, X. F.: Fast Nocturnal  
 Heterogeneous Chemistry in a Coastal Background Atmosphere and Its Implications for Daytime



559 Photochemistry, Journal of Geophysical Research-Atmospheres. 127,  
 560 <https://doi.org/10.1029/2022jd036716>, 2022.

561 Requia, W. J., Di, Q., Silvern, R., Kelly, J. T., Koutrakis, P., Mickley, L. J., Sulprizio, M. P., Amini, H.,  
 562 Shi, L. H., and Schwartz, J.: An Ensemble Learning Approach for Estimating High Spatiotemporal  
 563 Resolution of Ground-Level Ozone in the Contiguous United States, Environmental Science &  
 564 Technology. 54, 11037-11047, <https://doi.org/10.1021/acs.est.0c01791>, 2020.

565 Seinfeld, J. H.: URBAN AIR-POLLUTION - STATE OF THE SCIENCE, Science. 243, 745-752,  
 566 <https://doi.org/10.1126/science.243.4892.745>, 1989.

567 Sun, J. J., Qin, M. M., Xie, X. D., Fu, W. X., Qin, Y., Sheng, L., Li, L., Li, J. Y., Sulaymon, I. D., Jiang,  
 568 L., Huang, L., Yu, X. N., and Hu, J. L.: Seasonal modeling analysis of nitrate formation pathways in  
 569 Yangtze River Delta region, China, Atmospheric Chemistry and Physics. 22, 12629-12646,  
 570 <https://doi.org/10.5194/acp-22-12629-2022>, 2022.

571 Thaler, R. D., Mielke, L. H., and Osthoff, H. D.: Quantification of Nitryl Chloride at Part Per Trillion  
 572 Mixing Ratios by Thermal Dissociation Cavity Ring-Down Spectroscopy, Analytical Chemistry. 83,  
 573 2761-2766, <https://doi.org/10.1021/ac200055z>, 2011.

574 Tham, Y. J., Wang, Z., Li, Q. Y., Wang, W. H., Wang, X. F., Lu, K. D., Ma, N., Yan, C., Kecorius, S.,  
 575 Wiedensohler, A., Zhang, Y. H., and Wang, T.: Heterogeneous N<sub>2</sub>O<sub>5</sub> uptake coefficient and production  
 576 yield of ClNO<sub>2</sub> in polluted northern China: roles of aerosol water content and chemical composition,  
 577 Atmospheric Chemistry and Physics. 18, 13155-13171, <https://doi.org/10.5194/acp-18-13155-2018>,  
 578 2018.

579 Tham, Y. J., Wang, Z., Li, Q. Y., Yun, H., Wang, W. H., Wang, X. F., Xue, L. K., Lu, K. D., Ma, N., Bohn,  
 580 B., Li, X., Kecorius, S., Gröss, J., Shao, M., Wiedensohler, A., Zhang, Y. H., and Wang, T.: Significant  
 581 concentrations of nitryl chloride sustained in the morning: investigations of the causes and impacts on  
 582 ozone production in a polluted region of northern China, Atmospheric Chemistry and Physics. 16, 14959-  
 583 14977, <https://doi.org/10.5194/acp-16-14959-2016>, 2016.

584 Wagner, N. L., Riedel, T. P., Young, C. J., Bahreini, R., Brock, C. A., Dubé, W. P., Kim, S., Middlebrook,  
 585 A. M., Öztürk, F., Roberts, J. M., Russo, R., Sive, B., Swarthout, R., Thornton, J. A., VandenBoer, T. C.,  
 586 Zhou, Y., and Brown, S. S.: N<sub>2</sub>O<sub>5</sub> uptake coefficients and nocturnal NO<sub>2</sub> removal rates determined from  
 587 ambient wintertime measurements, Journal of Geophysical Research-Atmospheres. 118, 9331-9350,  
 588 <https://doi.org/10.1002/jgrd.50653>, 2013.

589 Wang, H. C., Lu, K. D., Chen, S. Y., Li, X., Zeng, L. M., Hu, M., and Zhang, Y. H.: Characterizing nitrate  
 590 radical budget trends in Beijing during 2013-2019, Science of the Total Environment. 795,  
 591 <https://doi.org/10.1016/j.scitotenv.2021.148869>, 2021.

592 Wang, H. C., Peng, C., Wang, X., Lou, S. R., Lu, K. D., Gan, G. C., Jia, X. H., Chen, X. R., Chen, J.,  
 593 Wang, H. L., Fan, S. J., Wang, X. M., and Tang, M. J.: N<sub>2</sub>O<sub>5</sub> uptake onto saline mineral dust: a potential  
 594 missing source of tropospheric ClNO<sub>2</sub> in inland China, Atmospheric Chemistry and Physics. 22, 1845-  
 595 1859, <https://doi.org/10.5194/acp-22-1845-2022>, 2022a.

596 Wang, H. C., Lu, K. D., Guo, S., Wu, Z. J., Shang, D. J., Tan, Z. F., Wang, Y. J., Le Breton, M., Lou, S.  
 597 R., Tang, M. J., Wu, Y. S., Zhu, W. F., Zheng, J., Zeng, L. M., Hallquist, M., Hu, M., and Zhang, Y. H.:  
 598 Efficient N<sub>2</sub>O<sub>5</sub> uptake and NO<sub>3</sub> oxidation in the outflow of urban Beijing, Atmospheric Chemistry and  
 599 Physics. 18, 9705-9721, <https://doi.org/10.5194/acp-18-9705-2018>, 2018.

600 Wang, H. C., Lu, K. D., Chen, X. R., Zhu, Q. D., Chen, Q., Guo, S., Jiang, M. Q., Li, X., Shang, D. J.,  
 601 Tan, Z. F., Wu, Y. S., Wu, Z. J., Zou, Q., Zheng, Y., Zeng, L. M., Zhu, T., Hu, M., and Zhang, Y. H.: High  
 602 N<sub>2</sub>O<sub>5</sub> Concentrations Observed in Urban Beijing: Implications of a Large Nitrate Formation Pathway,



Environmental Science & Technology Letters. 4, 416-420, <https://doi.org/10.1021/acs.estlett.7b00341>, 2017.

Wang, H. C., Yuan, B., Zheng, E., Zhang, X. X., Wang, J., Lu, K. D., Ye, C. S., Yang, L., Huang, S., Hu, W. W., Yang, S. X., Peng, Y. W., Qi, J. P., Wang, S. H., He, X. J., Chen, Y. B., Li, T. G., Wang, W. J., Huangfu, Y. B., Li, X. B., Cai, M. F., Wang, X. M., and Shao, M.: Formation and impacts of nitryl chloride in Pearl River Delta, Atmospheric Chemistry and Physics. 22, 14837-14858, <https://doi.org/10.5194/acp-22-14837-2022>, 2022b.

Wang, W. J., Li, X., Cheng, Y. F., Parrish, D. D., Ni, R. J., Tan, Z. F., Liu, Y., Lu, S. H., Wu, Y. S., Chen, S. Y., Lu, K. D., Hu, M., Zeng, L. M., Shao, M., Huang, C., Tian, X. D., Leung, K. M., Chen, L. F., Fan, M., Zhang, Q., Rohrer, F., Wahner, A., Pöschl, U., Su, H., and Zhang, Y. H.: Ozone pollution mitigation strategy informed by long-term trends of atmospheric oxidation capacity, Nature Geoscience. 16, 1080-1081, <https://doi.org/10.1038/s41561-023-01334-9>, 2023a.

Wang, Y. H., Gao, W. K., Wang, S., Song, T., Gong, Z. Y., Ji, D. S., Wang, L. L., Liu, Z. R., Tang, G. Q., Huo, Y. F., Tian, S. L., Li, J. Y., Li, M. G., Yang, Y., Chu, B. W., Petäjä, T., Kerminen, V. M., He, H., Hao, J. M., Kulmala, M., Wang, Y. S., and Zhang, Y. H.: Contrasting trends of PM<sub>2.5</sub> and surface-ozone concentrations in China from 2013 to 2017, National Science Review. 7, 1331-1339, <https://doi.org/10.1093/nsr/nwaa032>, 2020.

Wang, Y. R., Yang, X. Y., Wu, K., Mei, H., De Smedt, I., Wang, S. G., Fan, J., Lyu, S., and He, C.: Long-term trends of ozone and precursors from 2013 to 2020 in a megacity (Chengdu), China: Evidence of changing emissions and chemistry, Atmospheric Research. 278, <https://doi.org/10.1016/j.atmosres.2022.106309>, 2022c.

Wang, Y. T., Zhao, Y., Liu, Y. M., Jiang, Y. Q., Zheng, B., Xing, J., Liu, Y., Wang, S., and Nielsen, C. P.: Sustained emission reductions have restrained the ozone pollution over China, Nature Geoscience. 16, 967-+, <https://doi.org/10.1038/s41561-023-01284-2>, 2023b.

Wen, L., Xue, L. K., Wang, X. F., Xu, C. H., Chen, T. S., Yang, L. X., Wang, T., Zhang, Q. Z., and Wang, W. X.: Summertime fine particulate nitrate pollution in the North China Plain: increasing trends, formation mechanisms and implications for control policy, Atmospheric Chemistry and Physics. 18, 11261-11275, <https://doi.org/10.5194/acp-18-11261-2018>, 2018.

Wolfe, G. M., Marvin, M. R., Roberts, S. J., Travis, K. R., and Liao, J.: The Framework for 0-D Atmospheric Modeling (F0AM) v3.1, Geoscientific Model Development. 9, 3309-3319, <https://doi.org/10.5194/gmd-9-3309-2016>, 2016.

Xie, X. D., Hu, J. L., Qin, M. M., Guo, S., Hu, M., Wang, H. L., Lou, S. R., Li, J. Y., Sun, J. J., Li, X., Sheng, L., Zhu, J. L., Chen, G. Y., Yin, J. J., Fu, W. X., Huang, C., and Zhang, Y. H.: Modeling particulate nitrate in China: Current findings and future directions, Environment International. 166, <https://doi.org/10.1016/j.envint.2022.107369>, 2022.

Xing, J., Ding, D., Wang, S. X., Zhao, B., Jang, C., Wu, W. J., Zhang, F. F., Zhu, Y., and Hao, J. M.: Quantification of the enhanced effectiveness of NO<sub>x</sub> control from simultaneous reductions of VOC and NH<sub>3</sub> for reducing air pollution in the Beijing-Tianjin-Hebei region, China, Atmospheric Chemistry and Physics. 18, 7799-7814, <https://doi.org/10.5194/acp-18-7799-2018>, 2018.

Yan, C., Tham, Y. J., Nie, W., Xia, M., Wang, H. C., Guo, Y. S., Ma, W., Zhan, J. L., Hua, C. J., Li, Y. Y., Deng, C. J., Li, Y. R., Zheng, F. X., Chen, X., Li, Q. Y., Zhang, G., Mahajan, A. S., Cuevas, C. A., Huang, D. D., Wang, Z., Sun, Y. L., Saiz-Lopez, A., Bianchi, F., Kerminen, V. M., Worsnop, D. R., Donahue, N. M., Jiang, J. K., Liu, Y. C., Ding, A. J., and Kulmala, M.: Increasing contribution of nighttime nitrogen chemistry to wintertime haze formation in Beijing observed during COVID-19 lockdowns, Nature



647 Geoscience. 16, 975-+, <https://doi.org/10.1038/s41561-023-01285-1>, 2023.

648 Yang, C., Dong, H. S., Chen, Y. P., Xu, L. L., Chen, G. J., Fan, X. L., Wang, Y. H., Tham, Y. J., Lin, Z.  
649 Y., Li, M. R., Hong, Y. W., and Chen, J. S.: New Insights on the Formation of Nucleation Mode Particles  
650 in a Coastal City Based on a Machine Learning Approach, *Environmental Science & Technology*. 58,  
651 1187-1198, <https://doi.org/10.1021/acs.est.3c07042>, 2023.

652 Yang, S. X., Yuan, B., Peng, Y. W., Huang, S., Chen, W., Hu, W. W., Pei, C. L., Zhou, J., Parrish, D. D.,  
653 Wang, W. J., He, X. J., Cheng, C. L., Li, X. B., Yang, X. Y., Song, Y., Wang, H. C., Qi, J. P., Wang, B. L.,  
654 Wang, C., Wang, C. M., Wang, Z. L., Li, T. G., Zheng, E., Wang, S. H., Wu, C. H., Cai, M. F., Ye, C. S.,  
655 Song, W., Cheng, P., Chen, D. H., Wang, X. M., Zhang, Z. Y., Wang, X. M., Zheng, J. Y., and Shao, M.:  
656 The formation and mitigation of nitrate pollution: comparison between urban and suburban environments,  
657 *Atmospheric Chemistry and Physics*. 22, 4539-4556, <https://doi.org/10.5194/acp-22-4539-2022>, 2022.

658 Yu, C., Wang, Z., Xia, M., Fu, X., Wang, W. H., Tham, Y. J., Chen, T. S., Zheng, P. G., Li, H. Y., Shan,  
659 Y., Wang, X. F., Xue, L. K., Zhou, Y., Yue, D. L., Ou, Y. B., Gao, J., Lu, K. D., Brown, S. S., Zhang, Y.  
660 H., and Wang, T.: Heterogeneous N<sub>2</sub>O<sub>5</sub> reactions on atmospheric aerosols at four Chinese sites:  
661 improving model representation of uptake parameters, *Atmospheric Chemistry and Physics*. 20, 4367-  
662 4378, <https://doi.org/10.5194/acp-20-4367-2020>, 2020.

663 Yun, H., Wang, W. H., Wang, T., Xia, M., Yu, C., Wang, Z., Poon, S. C. N., Yue, D. L., and Zhou, Y.:  
664 Nitrate formation from heterogeneous uptake of dinitrogen pentoxide during a severe winter haze in  
665 southern China, *Atmospheric Chemistry and Physics*. 18, 17515-17527, [https://doi.org/10.5194/acp-18-](https://doi.org/10.5194/acp-18-17515-2018)  
666 [17515-2018](https://doi.org/10.5194/acp-18-17515-2018), 2018.

667 Zhai, S. X., Jacob, D. J., Wang, X., Liu, Z. R., Wen, T. X., Shah, V., Li, K., Moch, J. M., Bates, K. H.,  
668 Song, S. J., Shen, L., Zhang, Y. Z., Luo, G., Yu, F. Q., Sun, Y. L., Wang, L. T., Qi, M. Y., Tao, J., Gui, K.,  
669 Xu, H. H., Zhang, Q., Zhao, T. L., Wang, Y. S., Lee, H. C., Choi, H., and Liao, H.: Control of particulate  
670 nitrate air pollution in China, *Nature Geoscience*. 14, 389-+, [https://doi.org/10.1038/s41561-021-00726-](https://doi.org/10.1038/s41561-021-00726-z)  
671 [z](https://doi.org/10.1038/s41561-021-00726-z), 2021.

672 Zhai, T. Y., Lu, K. D., Wang, H. C., Lou, S. R., Chen, X. R., Hu, R. Z., and Zhang, Y. H.: Elucidate the  
673 formation mechanism of particulate nitrate based on direct radical observations in the Yangtze River  
674 Delta summer 2019, *Atmospheric Chemistry and Physics*. 23, 2379-2391, [https://doi.org/10.5194/acp-](https://doi.org/10.5194/acp-23-2379-2023)  
675 [23-2379-2023](https://doi.org/10.5194/acp-23-2379-2023), 2023.

676 Zhang, R., Han, Y. H., Shi, A. J., Sun, X. S., Yan, X., Huang, Y. H., and Wang, Y.: Characteristics of  
677 ambient ammonia and its effects on particulate ammonium in winter of urban Beijing, China,  
678 *Environmental Science and Pollution Research*. 28, 62828-62838, [https://doi.org/10.1007/s11356-021-](https://doi.org/10.1007/s11356-021-14108-w)  
679 [14108-w](https://doi.org/10.1007/s11356-021-14108-w), 2021.

680 Zhang, X., Ma, Q., Chu, W. H., Ning, M., Liu, X. Q., Xiao, F. J., Cai, N. N., Wu, Z. J., and Yan, G.:  
681 Identify the key emission sources for mitigating ozone pollution: A case study of urban area in the  
682 Yangtze River Delta region, China, *Science of the Total Environment*. 892,  
683 <https://doi.org/10.1016/j.scitotenv.2023.164703>, 2023a.

684 Zhang, Y., Lei, R., Cui, S., Wang, H., Chen, M., and Ge, X.: Spatiotemporal trends and impact factors of  
685 PM<sub>2.5</sub> and O<sub>3</sub> pollution in major cities in China during 2015-2020, *Chinese Science Bulletin*. 67, 2029-  
686 2042, 2022.

687 Zhang, Y. N., Wang, H. L., Huang, L. B., Qiao, L. P., Zhou, M., Mu, J. S., Wu, C., Zhu, Y. J., Shen, H.  
688 Q., Huang, C., Wang, G. H., Wang, T., Wang, W. X., and Xue, L. K.: Double-Edged Role of VOCs  
689 Reduction in Nitrate Formation: Insights from Observations during the China International Import Expo  
690 2018, *Environmental Science & Technology*. 57, 15979-15989, <https://doi.org/10.1021/acs.est.3c04629>,



2023b.

Zhao, S. P., Yin, D. Y., Yu, Y., Kang, S. C., Qin, D. H., and Dong, L. X.: PM<sub>2.5</sub> and O<sub>3</sub> pollution during 2015-2019 over 367 Chinese cities: Spatiotemporal variations, meteorological and topographical impacts, *Environmental Pollution*. 264, <https://doi.org/10.1016/j.envpol.2020.114694>, 2020.

Zhao, X. X., Zhao, X. J., Liu, P. F., Chen, D., Zhang, C. L., Xue, C. Y., Liu, J. F., Xu, J., and Mu, Y. J.: Transport Pathways of Nitrate Formed from Nocturnal N<sub>2</sub>O<sub>5</sub> Hydrolysis Aloft to the Ground Level in Winter North China Plain, *Environmental Science & Technology*. <https://doi.org/10.1021/acs.est.3c00086>, 2023.

Zhou, M., Nie, W., Qiao, L. P., Huang, D. D., Zhu, S. H., Lou, S. R., Wang, H. L., Wang, Q., Tao, S. K., Sun, P., Liu, Y. W., Xu, Z., An, J. Y., Yan, R. S., Su, H., Huang, C., Ding, A. J., and Chen, C. H.: Elevated Formation of Particulate Nitrate From N<sub>2</sub>O<sub>5</sub> Hydrolysis in the Yangtze River Delta Region From 2011 to 2019, *Geophysical Research Letters*. 49, <https://doi.org/10.1029/2021gl097393>, 2022.

Zong, Z., Tian, C. G., Sun, Z. Y., Tan, Y., Shi, Y. J., Liu, X. H., Li, J., Fang, Y. T., Chen, Y. J., Ma, Y. H., Gao, H. W., Zhang, G., and Wang, T.: Long-Term Evolution of Particulate Nitrate Pollution in North China: Isotopic Evidence From 10 Offshore Cruises in the Bohai Sea From 2014 to 2019, *Journal of Geophysical Research-Atmospheres*. 127, <https://doi.org/10.1029/2022jd036567>, 2022.